Spectroscopic, Structural and DFT Study of the Responses of Carbonylmetal Crown Ether Complexes to Alkali Metal Cations

ARTICLE *in* BERICHTE DER DEUTSCHEN CHEMISCHEN GESELLSCHAFT · MAY 2011

Impact Factor: 2.94 · DOI: 10.1002/ejic.201001274

4 AUTHORS:

G.Richard Stephenson
University of East Anglia
167 PUBLICATIONS **2,140** CITATIONS
SEE PROFILE

Christopher Anson
Karlsruhe Institute of Technology
323 PUBLICATIONS **7,979** CITATIONS
SEE PROFILE

Colin Creaser
Loughborough University
175 PUBLICATIONS **2,955** CITATIONS
SEE PROFILE

Claude Daul
Université de Fribourg
118 PUBLICATIONS **2,241** CITATIONS
SEE PROFILE

Spectroscopic, Structural and DFT Study of the Responses of Carbonylmetal Crown Ether Complexes to Alkali Metal Cations

G. Richard Stephenson,*[a] Christopher E. Anson,[b] Colin S. Creaser,[c] and Claude A. Daul[d]

Keywords: Crown compounds / Alkali metal ions / IR spectroscopy / Density functional calculations / Molecular sensors / Carbonyl ligands

FTIR spectra of tricarbonyl(η^6-benzo-15-crown-5)chromium(0) (**1**) in the presence of lithium, sodium and potassium perchlorate salts in methanol show different responses in the Cr–CO vibrational region of the spectrum. Data from the symmetric (ν_{sym}) and antisymmetric (ν_{asym}) Cr–CO vibrational stretching modes have been analysed by principal component analysis (PCA) to generate a factor score plot that provides a visual representation of these differential responses. X-ray crystallographic data for the sodium perchlorate complex **1**·Na^+ and dimensions from DFT-derived structures of **1**·Li^+, **1**·Na^+ and **1**·K^+ indicate that binding M^+ in the crown causes electron density and structural changes in the [O(4)–C(9)–C(4)–O(8)]Cr–C(1)=O(1) sections of **1**, which vary depending on the nature of the cation. This suggests a mode of action in which Li^+ associates with a more compact O(4)–C(9)–C(4)–O(8), while Na^+ and K^+ differ crucially in the extent of σ and π contributions to their effect on ν_{sym} and ν_{asym}. A comparison of the FTIR data from **1**, tricarbonyl(η^6-1-phenyl-1-aza-15-crown-5)chromium(0) (**2**) and tricarbonyl(η^6-2-phenyl-15-crown-5)chromium(0) (**3**) with a wider range of cations (NH_4^+, Li^+, Na^+, K^+, Rb^+, Cs^+, Mg^{2+}, Ba^{2+}) and anions (AcO^-, BPh_4^-, Br^-, $C1O_4^-$, I^-, SCN^-), showed that **1** and **3** both responded significantly to the different metal cations, but **2** did not. The relative cation differentiation of **1**, **2** and **3** was measured using the parameter $\Delta_{R(cation)}$, and ratios of $\Delta_{N(cation)}$ values [calculated from $\Delta_{R(cation)}$] distinguished different effects in the FTIR spectra of **1** and **3** for different pairs of cations.

Introduction

Carbonylmetal complexes offer fundamental advantages when employed as reporting groups in molecular sensors. Their spectra contain more information than is available from other more conventional readout strategies.[1,2] The narrow symmetric (ν_{sym}) and antisymmetric (ν_{asym}) vibrational stretching modes respond to the distribution of charge between the metal and the carbonyl ligands (an electronic effect). Additional information is available from vibrational coupling which is influenced by conformational changes in the geometry of the arrangement of the ligands around the metal (a structural effect). The widths of the vibrational bands also contain information, and are influenced, for example, by solvent polarity (an environment effect). In tricarbonylmetal complexes, there are two antisymmetric bands, which are often degenerate, but when the complex is unsymmetrical, a second vibrational coupling separates the antisymmetric bands. Although usually not resolved, the separation of these two overlapping vibrationally coupled modes broadens the band envelope. Thus the width of the antisymmetric band envelope is sensitive both to environmental effects and structural effects. We have shown in a study of solvent effects on supported metal complexes that principal component analysis (PCA) is a good way to visualise subtle changes in the spectra.[3]

Tricarbonylchromium derivatives of benzocrown ethers have been available[4–7] for many years, and we have shown[8] that sodium ion concentrations in the range 5–35 mM can be measured from the IR spectra of tricarbonyl(η^6-benzo-15-crown-5)chromium (**1**). The possibility of competing interactions from Li^+, Na^+ and K^+ is a classic problem in the development of sensors for alkali metal ions, since all three ions bind easily (though to different extents) to the crown ether, and much effort has been devoted by many research groups to the development of molecular sensors for Li^+, Na^+ and K^+.[9] The high information content intrinsic to the IR readout method, however, provides the key to solving this problem, and we describe here the use of PCA with lithium, sodium and potassium perchlorate salts, within a simple crown ether receptor bearing the tricarbonylchromium moiety as the reporting group.

[a] School of Chemistry, University of East Anglia,
Norwich, NR4 7TJ, UK
Fax: +44-1603-592003
E-mail: g.r.stephenson@uea.ac.uk
[b] Institut für Anorganische Chemie, Karlsruhe Institute of Technology,
Engesserstr. Geb. 30.45, 76128 Karlsruhe, Germany
[c] Centre for Analytical Science, Department of Chemistry, Loughborough University,
Loughborough, LE11 3TU, UK
[d] Department of Chemistry, University of Fribourg,
1700 Fribourg, Switzerland

Results and Discussion

The crystal structure of **1**·Na^+ as the SCN^- salt[8] shows the 15-crown-5 complex to be well suited for sodium ion detection, as the crown is tilted slightly downwards towards the $Cr(CO)_3$ group, and the sodium ion, which lies slightly above the five oxygen atoms of the crown, is aligned in the correct fashion to interact with the two oxygen atoms on the aromatic ring. This thiocyanate salt, however, showed a distorted structure with strong coordination of the sodium ion by SCN^-, making interpretation difficult because of the possibility that this might significantly affect the position of the metal relative to the oxygen atoms in the crown. Crystals with the less strongly coordinating perchlorate anion have now been studied for comparison (Figure 1, a). The resulting structure is unusual, with two ClO_4^- anions present as a dimeric bridge between two (η^6-benzo-15-crown-5)$Cr(CO)_3Na^+$ units related by a crystallographic centre. The conformation of the crown identified in the perchlorate salt shows a significantly better alignment of the metal cation which lies further from the crown, and almost in the plane of the aromatic ring [the dihedral angle between the Na–O(4)–O(8) plane and the mean plane through the $C_6H_4O_2$ unit is only 2.9° compared to 10.7° in the SCN^- case]. If the crystallographically defined position of the Na^+ is also significant in solution, **1** should be well suited to demonstrate the power of PCA with mixtures of Li^+, Na^+ and K^+ perchlorate salts (perchlorates were chosen minimise covalent interactions between anion and cation and to ensure good solubility in methanol). In methanol solution, especially with the weakly associating perchlorate ion, coordination by MeOH is likely to replace the anion binding characterised in the crystal structure, but the overall conformation of the crown should remain sufficiently similar for good electronic communication between the metal cation and the $Cr(CO)_3$ group to be retained.

For the PCA study, a set of sixteen methanol solutions of $LiClO_4$, $NaClO_4$ and $KClO_4$ were prepared with different ratios (4:0:0, 3:1:0, 2:2:0, 2:1:1, etc) with the total metal ion concentration at 20 mM in each case. Complex **1** (Figure 2) was included at 2.25 mM. FTIR spectra were recorded at 0.5 cm^{-1} resolution using a 0.5 cm pathlength solution cell and were normalised in the vertical scale (Figure 3). The best PCA results (SPSS-X) were obtained from analysis of spectroscopic data in the range 1890–1880 cm^{-1}, which corresponds to the top of the antisymmetric band envelope where the different profiles are well separated. The factor score plot (Figure 4) shows the expected triangular form, with the data for each 4:0:0 ratio (i.e. for Li^+, Na^+ or K^+ only in the sample) at each corner. Binary mixtures are well resolved on the sides of the diagram, and ternary mixtures (i.e. 2Li^+:Na^+: K^+; Li^+:2Na^+: K^+; Li^+:Na^+:2 K^+) lie within these boundaries. The 1:1:1 ternary mixture corresponds to the central position on the factor score plot within the region identified by the 2:1:1 data. The best-fit line through the points for a series of measurements for a binary mixture of two metal ions should not have a contribution to its fac-

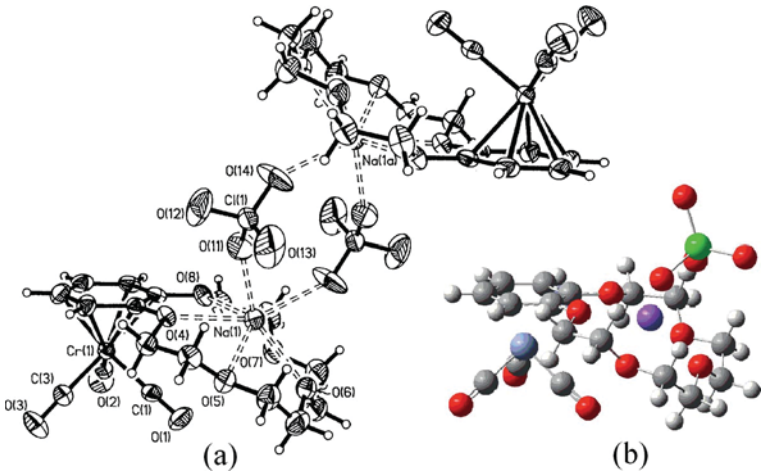

Figure 1. a: ORTEP drawing of the X-ray structure of [(**1**·Na^+) $C1O_4^-$]$_2$; b: corresponding view of the optimised structure (b3ylp/Lanl2DZ) from DFT calculations.

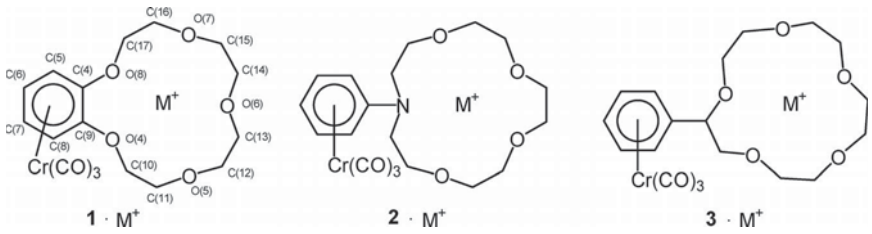

Figure 2. Metal cation adducts of tricarbonylchromium derivatives **1**, **2** and **3** of crown ethers (atom labels on **1** correspond to numbering in the X-ray structure).

tor scores from the third metal ion. This was assessed by recalculating each binary trend-line including data for the 1:1:1 point. In all three cases, this caused substantial worsening of the root mean square (RMS) fit [the RMS value increased by a factor of 1.5 (adding K^+ to the Li^+, Na^+ line), 3.8 (adding Li^+ to the Na^+, K^+ line) and 5.2 (adding Na^+ to the Li^+, K^+ line)], indicating that the 1:1:1 point was significantly different to the data points for the binary mixtures. Finally, using the learning set defined by these sixteen samples, the factor scores for 2.25 mM **1** (i.e. the empty crown) were calculated from a normalised spectrum. These factor scores gave a point which lay outside the triangle, close to, but not coincident with, the "4Li" point. This pattern of factor scores provides a good approach to visualise the qualitative differences apparent in the spectra illustrated in Figure 3.

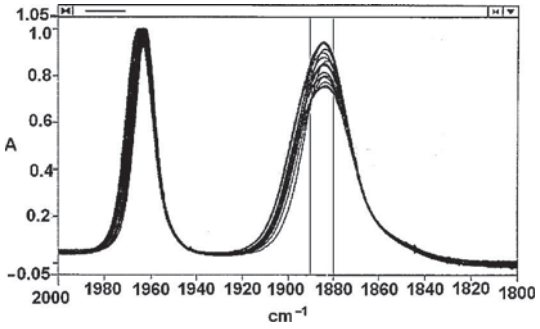

Figure 3. Normalised FTIR spectra of **1** in methanol in the presence of mixtures of lithium, sodium and potassium perchlorate salts.

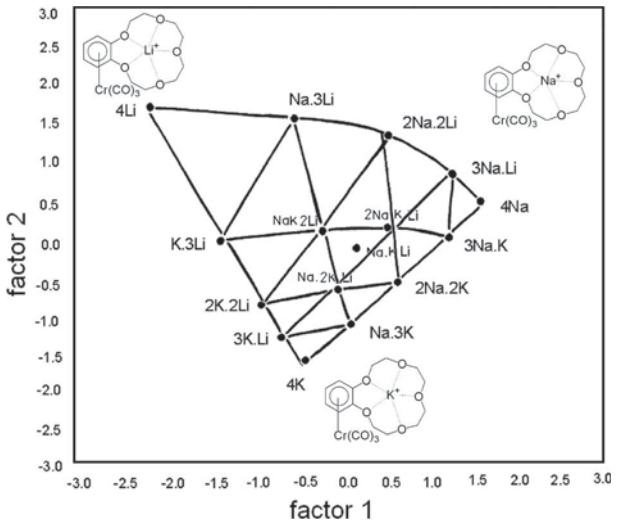

Figure 4. PCA factor score plot of spectroscopic data in the range 1890–1880 cm^{-1} from Figure 3.

As a further check of the ability of the FTIR method to identify the presence of an alkali metal cation in the crown, the response to a series of different cation concentrations was examined in the crystallographically defined sodium ion case. A range of methanol solutions, all 1.4 mM in **1** but with concentrations of $Na(C1O_4)$ varying from 0 to 100 mM, were prepared and their FTIR spectra recorded. The spectra, shown in Figure 5 (a), demonstrate good isosbestic points, providing evidence that only the empty crown and the structurally characterised 1:1 adduct were present. The wavenumbers of the band maxima for the $\nu_{sym}(CO)$ and $\nu_{asym}(CO)$ modes were measured and are plotted against $[Na^+]$ in Figure 5 (b). As the sodium ion concentration increases, the $\nu_{sym}(CO)$ and $\nu_{asym}(CO)$ peaks for **1**·Na^+ grow progressively taller as the proportion of the crown associated with the cation becomes greater. There is also a slight but measurable shift to higher wavenumbers in the maxima for the $\nu_{sym}(CO)$ and $\nu_{asym}(CO)$ modes for **1**·Na^+ at higher $[Na^+]$. This is illustrated in Figure 5 (a) in the expansion of the stack of the four highest $\nu_{asym}(CO)$ bands which correspond to the last four data points in the gradually rising final section of the lower curve in Figure 5 (b) (35–100 mM) where a series of small but incremental increases in the vibrational frequency are apparent.

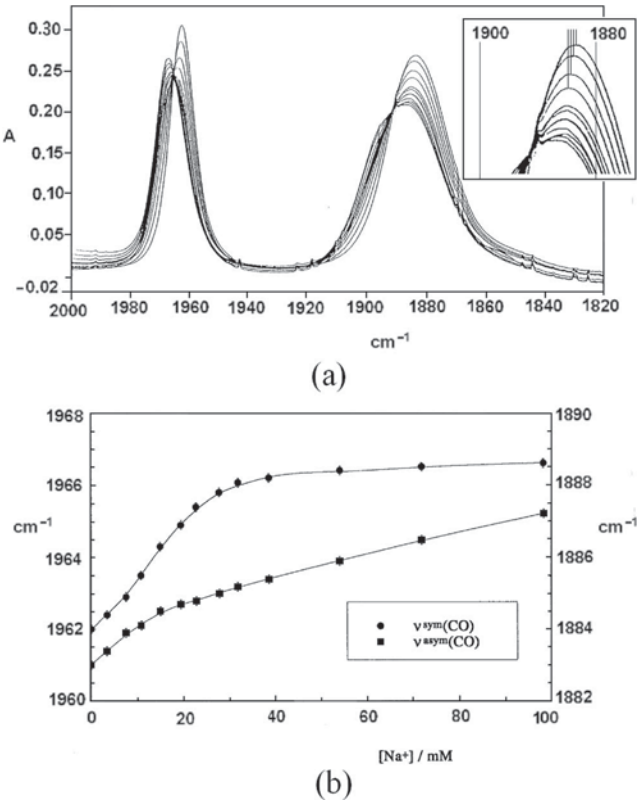

Figure 5. a: Superimposed FTIR spectra for **1**·Na^+ with $[Na^+]$ varying from 0 to 98 mM [inset: expansion of the maxima observed for $\nu_{asym}(CO)$]; b: positions of ν_{max} for the $\nu_{sym}(CO)$ and $\nu_{asym}(CO)$ stretching vibrations plotted against $[Na^+]$.

To explore the origins of these different spectroscopic responses, **1** was compared with **2** and **3**,[10] and a wider range of cations (NH_4^+, Li^+, Na^+, K^+, Rb^+, Cs^+, Mg^{2+}, Ba^{2+}). Complexes **2** and **3** were prepared by heating the appropriate ligand with hexacarbonylchromium in a di-*n*-butyl ether/THF mixed solvent system. In order to reach a limiting spectrum with a high level of occupancy of the crown, a 100-fold excess of the metal cation was used (tricarbonylchromium complex at 2 mM; metal cation at 200 mM). The

Table 1. Data from FTIR spectra of **1** (corresponding data for **2** and **3** are provided in the Supporting Information) (the estimation of errors is indicated in footnotes).

		$\nu_M(max)$[a] [cm^{-1}]		$\nu_M(max)$[a] – $\nu_0(max)$[b] [cm^{-1}]			Width[c] [cm^{-1}]	$\Delta_{R(cation)}$ [d]
	1·M^+	ν_{sym}	ν_{asym}[e]	$\Delta\nu_{sym}$	ν_{asym}[e]	sym	asym[e]	
1	–[b]	1962.0[f]	1882.2[f]	–	–	10.1[g]	23.4[g]	–
2	NH_4^+	1963.0[f]	1883.7[f]	+1.0[g]	+1.5[g]	10.7[g]	27.0[g]	1.80[h]
3	Li^+	1962.2[f]	1882.5[f]	+0.2[g]	+0.3[g]	11.2[g]	25.5[g]	0.36[h]
4	Na^+	1966.5[f]	1887.3[f]	+4.5[g]	+5.1[g]	11.2[g]	29.3[g]	6.80[h]
5	K^+	1964.3[f]	1884.3[f]	+2.3[g]	+2.1[g]	10.5[g]	31.9[g]	3.11[h]
6	Rb^+	1964.3[f]	1883.7[f]	+2.3[g]	+1.5[g]	10.5[g]	32.7[g]	2.75[h]
7	Cs^+	1964.0[f]	1883.2[f]	+2.0[g]	+1.0[g]	10.7[g]	32.2[g]	2.24[h]
8	Mg^{2+}	1961.6[f]	1881.3[f]	–0.4[g]	–0.9[g]	10.5[g]	24.6[g]	0.89[h]
9	Ba^{2+}	1968.1[f]	1887.2[f]	+6.1[g]	+5.0[g]	13.2[g]	40.2[g]	
10	Ba^{2+}[i]	1968.9						8.52[j]

[a] Frequencies of $Cr(CO)_3$ vibrational stretching modes in methanol by FTIR. [b] Measured for the empty crown without M^+ present. [c] Width at half height. [d] Calculated from the diagonal separation on the Bellamy plot (Figure 6) as defined in ref.[16] [e] Data determined from two unresolved vibrational modes from the mid-point between the positions on either side of the band at the points where the absorbance was half that at the band maximum. [f] Linear regression lines determined for the plots of ν_{sym} and ν_{asym} of **1** against $[Na^+]$ at low (1–20 mM) sodium ion concentrations were used to calculate $S_{y/x}$ (for ν_{sym}: ±0.15; ν_{asym}: ±0.12) in measurements of the position of $\tilde{\nu}_{max}$ (see Supporting Information). [g] For ν_{sym}: ±0.21; ν_{asym}: ±0.16. [h] ±0.15. [i] Vibrational frequency identified using the curve-fitting programme PCCAP. [j] Calculated using ν_{sym} = 1968.9 cm^{-1} (the antisymmetric band could not be separated accurately into its four components by PCCAP, so the value of 1887.2 cm^{-1} was used).

results for **1**, **2** and **3** are presented in Table 1 (**1**) and in the Supporting Information (**2** and **3**), together with data for the empty crowns. It can be seen that there is considerable variation in the positions of the symmetric and antisymmetric bands. The expectation is that binding a metal cation in the crown influences charge distribution in the complex in much the same way as has been observed[11] for hydrogen bonding at pyrazine ligands in $Cr(CO)_5$ complexes, for dissociation of carboxylic acid substituents on ligands in $Fe(CO)_3$ and $Cr(CO)_3$ complexes,[12] and in an electrochemical investigation[13] of $W(CO)_5$(azaferrocene) adducts with potential applications as IR-detectable tracers for amino groups. In previous studies[14] we have found that Bellamy plots[15] are a convenient method to depict results of this type. The plots for complexes **1**, **2** and **3** (Figure 6) show the normal linear trend. The azacrown Cr–CO vibrational bands appear at lower wavenumbers as a consequence of electron donation from the adjacent nitrogen atom, and are bunched together on the Bellamy plot; complex **2** is poor at discriminating between the metal cations used in the study. Complex **3** was chosen because the (η^6-Ph)$Cr(CO)_3$ section is not in direct electronic communication with the heteroatoms of the crown, however, unexpectedly, Figure 6 shows that complex **3** gives a substantial range of responses to the different cations. The spread of data points along the diagonal gives an indication of the extent of differentiation in the spectroscopic responses, and this is similar for complexes **1** and **3**. Electron donation into the (η^6-Ar)$Cr(CO)_3$ complex from the adjacent oxygen atoms also lowers the vibrational frequencies of the Cr–CO stretching modes of **1**, but not to the same extent as in the azacrown case. The nitrogen atom in complex **3** donates more electron density to the chromium complex than the two oxygen atoms in **1**, and from the spectroscopic data it can be seen that the electron density on the $Cr(CO)_3$ group is in the order **2** > **1** > **3**. We have previously defined a measure (Δ_R, based on the diagonal separation of the extremes of each Bellamy plot) to give a quantitative guide to the range of responses possible with each metal complex.[14,16] $\Delta_{R(cation)}$ values based on this approach are presented in Table 1 and in the Supporting Information. This data shows that the capability to discriminate between NH_4^+, Li^+, Na^+, K^+, Rb^+, Cs^+, Mg^{2+} and Ba^{2+} is in the order **1**, **3** > **2** and for complexes **1** and **3**, the strength of the effect of the metal cations varies in the sequence $Ba^{2+} > Na^+ > K^+$, Cs^+, $Rb^+ > Mg^{2+}$, Li^+. Table 1 (line 9) also shows that the spectrum measured for Ba^{2+} with **1** has far broader vibrational bands than the others. Such broadening can be a consequence of the presence of two species in solution, suggesting that even with 100-fold excess of the metal ion, the crown ether may not be fully occupied. Analysis of ν_{sym} in this spectrum using the curve-fitting programme PCCAP[17] indicated the presence of two overlapping bands in a roughly 3:1 ratio. The major contribution came from a stretching vibration at 1968.9 cm^{-1}, which was present in the spectrum together with the ex-

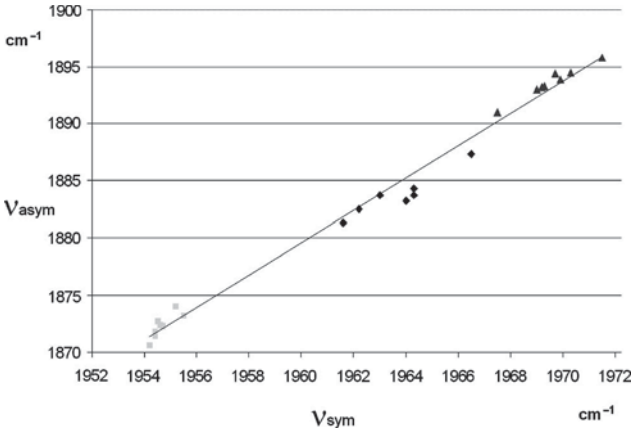

Figure 6. Bellamy plots of the frequencies of the symmetric and asymmetric Cr–CO vibrational modes of **2** (squares), **1** (diamonds) and **3** (triangles); the trend line is from the data for all three complexes (the data point for **1**·Ba^{2+} was excluded).

$$\Delta_{N(\text{complex X})} = \frac{\Delta_{R(\text{cation n})(\text{complex X})} - \Delta_{R(\text{cation m})(\text{complex X})}}{\Delta_{R(Ba^{2+})(\text{complex X})}} \quad (1)$$

pected vibration for the empty crown. The value observed for **1**·Ba^{2+} directly from the spectrum and the corrected value from curve-fitting are similar. The data supports the conclusion that binding Ba^{2+} has the greatest effect on shifting the Cr–CO vibrations of **1** to higher wavenumbers.

The parameter Δ_N has been developed[16] to give an indication of the relative distributions of individual responses on the diagonal of the Bellamy plot, and so aid the comparison of the relative performance of two metal complexes as sensors to differentiate several analytes. The Δ_N for a complex is calculated to show the magnitude of the difference in its responses to two solvents[16] or analytes, as a ratio against the largest response measured for the complex. Thus for any pair of analytes, Δ_N is a measure of the relative level of the response. This allows several complexes to be compared by calculating the ratio of Δ_N values. Equation (1) shows the method of calculation of $\Delta_{N(\text{cation})}$ values used in this study, in which Ba^{2+} gave the largest shifts of ν_{sym} and ν_{asym} compared to the empty crown.

To compare **1** and **3** for the range of metal ions NH_4^+, Li^+, Na^+, K^+, Rb^+, Cs^+, Mg^{2+} and Ba^{2+}, ratios of $\Delta_{N(\text{cation})}$ values are calculated for each pair of ions in turn. A three-dimensional plot of this data (Figure 7, a) shows a series of maxima and minima distributed about the mean value (1.16 in the case of complexes **1** and **3**) for the entire set of ratios. The vertical axis indicates the difference in the extent of differentiation of each pair of ions by the two complexes, and the edges of the horizontal plane correspond to the grid of metal ions compared in the plot (i.e. each horizontal intersection corresponds to a pairwise comparison of the relative effects of two cations). It can be seen from Figure 7 (a) that complexes **1** and **3** perform similarly in their ability to distinguish most pairs of metal ions, but there are several notable differences in which complex **1** significantly outperforms complex **3** and consequently the ratio $\Delta_{N(1)}/\Delta_{N(3)}$ is large [$\Delta_{N(1)}/\Delta_{N(3)}$ = +6.96 for Na^+ and NH_4^+; +5.39 for Rb^+ and Li^+; +3.32 for K^+ and Na^+; +2.08 for Na^+ and Li^+; –3.35 for K^+ and NH_4^+; –2.31 for Cs^+ and Rb^+]. For example, **1** responds significantly to Na^+ but much less to NH_4^+ [$\Delta_{N(1)}/\Delta_{N(3)}$ at +6.96 is the largest value in Figure 7, a]. ν_{sym} in the presence of 200 mM Na^+ is shifted to 1966.5 cm^{-1} compared to that of the empty crown (1962.0 cm^{-1}), an increase in vibrational frequency of 4.5 cm^{-1}. The effect of NH_4^+ is much smaller (an increase of only 1.0 cm^{-1}). The shifts in ν_{asym} follow the same pattern. For **3**, however, both cations increase the vibrational frequency by a similar (though smaller) amount ($\Delta\nu_{sym}$: 2.5 cm^{-1} for Na^+ and 1.9 cm^{-1} for NH_4^+; $\Delta\nu_{asym}$ 2.7 cm^{-1} for Na^+ and 2.6 cm^{-1} for NH_4^+). This approach provides a way to screen[16] complexes for use in dual sensor procedures.[18] To perform well for a given pair of analytes, high magnitudes for Δ_N and Δ_R are needed. Complex **1** also shows a large magnitude of response for Na^+ (Δ_R = 6.8). Some of the ratios displayed in Figure 7 (a) are negative values. For example, for **3**, ν_{asym} is influenced to a greater extent by NH_4^+ than K^+ (a shift of 2.6 cm^{-1} for NH_4^+ and 2.1 cm^{-1} for K^+) whereas both cations have almost the same effect on ν_{sym} ($\Delta\nu_{sym}$ is 1.9 cm^{-1} for NH_4^+ and 2.1 cm^{-1} for K^+). The antisymmetric band envelope contains information about vibrational coupling between the carbonyl ligands, and so can respond differently to ν_{sym}. This comparison provides a good example of the additional information in the IR spectra of tricarbonylmetal complexes, which makes PCA possible.

There are also pairs of metal ions where **3** outperforms **1** (Figure 7, b). For example, **3** responds relatively strongly

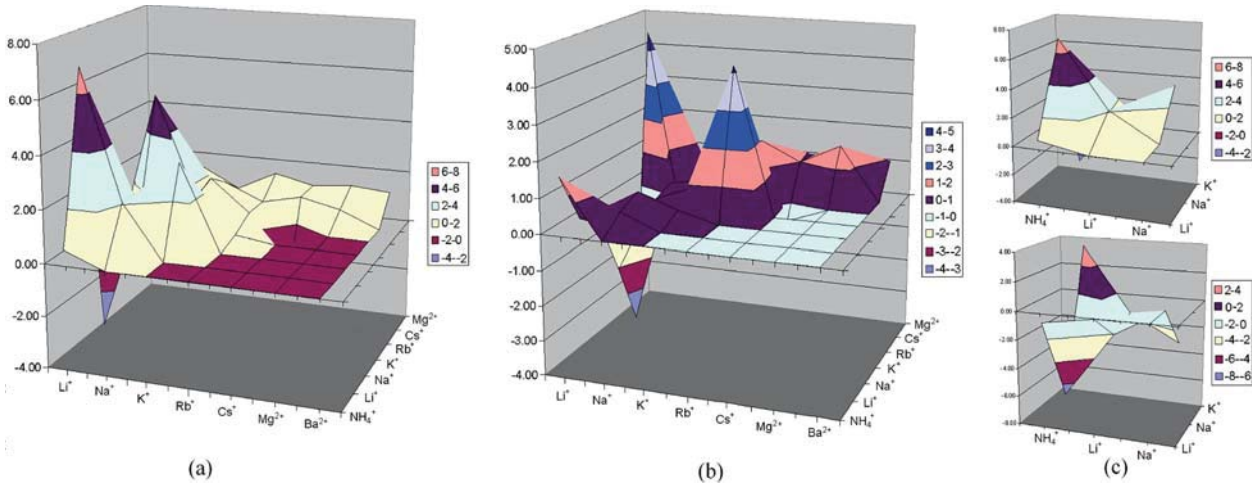

Figure 7. Plots of ratios of Δ_N values (vertical axes) for pairs of M^+ ions [a: $\Delta_{N(1)}/\Delta_{N(3)}$; b: $\Delta_{N(3)}/\Delta_{N(1)}$; c: two views of $\Delta_{N(1)}/\Delta_{N(3)}$ data from (a) to compare responses of **1** and **3** to NH_4^+ and the three alkali metal cations Li^+, Na^+ and K^+ giving the PCA data in Figure 4].

to NH_4^+ and less so to Mg^{2+} and Cs^+. Similarly, comparing the effects of K^+ and Rb^+ on ν_{sym} shows that **3** is more strongly influenced by K^+ than Rb^+ (shifts of 2.1 cm^{-1} for K^+ and 1.4 cm^{-1} for Rb^+) but for **1**, the shifts in vibrational frequencies are the same (2.3 cm^{-1}). The same difference in the responses in this case is also present in the antisymmetric vibration. The patterns of differential responses identified in Figure 7 in plots of Δ_N ratios can guide the design of dual sensor approaches to improve the discrimination of competing effects. Figure 7 (c) shows two views of a subset (for NH_4^+, Li^+, Na^+, K^+) of data from Figure 7 (a). Complex **3** lacks direct electronic communication between the heteroatoms in the crown and the arene ligand of the $Cr(CO)_3$ complex, and so responds in a significantly different way to the presence of cations in the crown. This suggests that the PCA approach (Figure 4) to distinguish Li^+, Na^+ and K^+ can be extended by including spectroscopically complementary η^n-carbonylmetal crown derivatives in which the η^n ligand is attached at one of the carbon atoms in the crown. The high level of shifts ($\Delta\nu_{sym}$ and $\Delta\nu_{asym}$) in the vibrational bands of **3** is an unexpected conclusion from the data presented in Table 1 and Table S1 (Supporting Information), and suggests a rational approach to extend the PCA methods reported here with procedures employing dual carbonylmetal probes.

Although the PCA study employed a common counterion (perchlorate), a selection of different counterions were present in the comparison of Δ_R and Δ_N data for NH_4^+, Li^+, Na^+, K^+, Rb^+, Cs^+, Mg^{2+} and Ba^{2+}. Using salts of Li^+, Na^+ and K^+ with **1**, the effects of counterions have been compared (Table 2) and shown to be small compared the effects of the cations. FTIR spectra of **1** and tricarbonyl(η^6-1,2-dimethoxybenzene)chromium(0) (**4**) were measured in methanol solutions containing a range of lithium, sodium and potassium salts: LiBr, $LiClO_4$, $LiBPh_4$, NaOAc, NaBr, NaSCN, $NaClO_4$, $NaBPh_4$, KOAc, KI and KSCN. Each solution was 2 mM in the chromium complex and 200 mM in the metal salt. Clearly, it would have been more systematic to have used all three metal salts of a given anion; however, some of these salts are insufficiently soluble in methanol. This range of salts is adequate for the investigation of the anion dependence. Table 2 and Table S2 (see Supporting Information), show the wavenumber shifts and bandwidths for the ν_{sym}(CO) and ν_{sym}(CO) modes of **1** in the different salt solutions. It is immediately apparent that any anion dependence of the shifts in ν(CO) is very slight, and much smaller than the differences between the shifts induced by the different metal cations. The tetraphenylborate anion behaves differently to the other anions, raising the possibility that a π stacking interaction takes place between one of the electron-rich phenyl rings and the *exo*-face of the (η^6-$C_6H_4O_2$) ring. We have characterised[19] such interactions by FTIR spectroscopy, and found that they result in small shifts for the ν(CO) modes, comparable to those observed for the BPh_4^- anion and the more accessible aromatic ring of complex **4** (Δν: –1.3 to –2.4 cm^{-1}). The effect of anions on **3** was also tested, and the BPh_4^- anion was again found to behave differently to the others. Data for **3** and **4** are presented in the Supporting Information. In all the cases examined, the differences in vibrational frequencies resulting from the presence of different cations far exceeds the differences caused by the choice of anion.

The crystal structure of **1**·Na^+ ClO_4^- shows the anticipated coordination of the sodium cation within the crown.[20] The bond lengths from Na(1) to O(6), O(7) and O(8) (2.468, 2.416 and 2.431 Å, respectively) are similar to those found[21,22] for sodium adducts of the free benzo-15-crown-5. In contrast, the Na–O bond lengths to the oxygen atoms O(4) and O(8) are longer at 2.509 and 2.508 Å. This was not the case in our earlier structure of the thiocyanate salt [bond lengths to oxygen atoms O(4): 2.442; O(8): 2.422; O(5): 2.397; O(7): 2.414; O(6): 2.351 Å],[8] where all the distances were similar, with Na–O(6) at the far end of the crown slightly shorter than the others. The perchlorate salt has Na–O(7) shorter than Na–O(5), showing that the sodium ion is displaced slightly towards the far side of the crown, when viewed as depicted in Figure 1 (a). This is presumably a consequence of the presence of the unusual bridging pair of perchlorate anions distorting the structure. This issue was addressed by DFT calculations[23,24] using the b3ylp functional and the Lanl2DZ basis set to optimise a monomeric perchlorate structure in the gas phase (Figure 1, b). A frequency calculation confirmed that the optimised geometry was an energy minimum. The conformation of the crown was very similar to that defined by crystallography, with an alternating up-down pattern of oxygen

Table 2. Shifts (Δν) in the position of ν(CO) bands of **1** as a 2 mM solution in methanol, calculated by subtracting the peak position recorded with 200 mM salt present from that recorded in pure methanol.

M^+	IR mode $\nu_M(max)$[b] – $\nu_0(max)$[d]	X^- AcO^- [cm^{-1}]	Br^-/ I^-[c] [cm^{-1}]	SCN^- [cm^{-1}]	ClO_4^- [cm^{-1}]	Range[a] [cm^{-1}]	X^- BPh_4^- [cm^{-1}]
Li^+	$\Delta\nu_{sym}$	–	+0.2[e]	–	+0.2[e]	0.0[g]	+0.4[e]
Li^+	$\Delta\nu_{asym}$	–	+0.2[f]	–	+0.3[f]	0.1[h]	+0.4[f]
Na^+	$\Delta\nu_{sym}$	+4.6[e]	+4.6[e]	+4.5[e]	+4.5[e]	0.1[g]	+3.2[e]
Na^+	$\Delta\nu_{asym}$	+5.5[f]	+5.4[f]	+5.3[f]	+5.1[f]	0.4[h]	+3.9[f]
K^+	$\Delta\nu_{sym}$	+2.6[e]	+2.3[e]	+2.4[e]	–	0.3[g]	–
K^+	$\Delta\nu_{asym}$	+2.4[f]	+2.1[f]	+2.0[f]	–	0.4[h]	–

[a] Excluding BPh_4^-. [b] Frequencies of $Cr(CO)_3$ vibrational stretching modes in methanol by FTIR. [c] LiBr, NaBr, KI. [d] Measured for the empty crown without M^+ present (corresponding data for **3** and **4**, and band broadening in **1**, **3** and **4** are provided in the Supporting Information). [e] ± 0.21. [f] ± 0.16. [g] ± 0.30. [h] ± 0.23.

atoms relative to the mean plane of the crown [O(4), O(8) and the unique oxygen atom O(6) at the position furthest from the arene point up and O(5) and O(7) point down]. The sodium ion lies above the crown, well aligned with O(4) and O(8) which, as in the crystal structure, are sp^2 hybridised [this is clear from the C–O–C bond angles of 119° at O(4) and O(8)]. The Na–O bond lengths obtained by DFT (Table 3) show a more symmetrical pattern with Na–O(6) now the shortest. The distances to O(5) and O(7) which point down were slightly longer than the others. The perchlorate ion was present in a chelating η^2 coordination mode which is consistent with the structure[21] of (benzo-15-crown-5)·$Na^+ClO_4^-$ which, unlike the tricarbonylchromium complex **1**·$Na^+ClO_4^-$, crystallised as a monomer. The same procedure was used to study structures with lithium and potassium ions coordinated by the crown, again as perchlorate salts (Table 3). Optimised geometries in which the perchlorate ions retained the chelating η^2 coordination to M^+ were again obtained but the frequency calculations revealed negative values; the structures obtained thus correspond to transition states between alternative conformations. With Li^+ in the crown, a monocoordinate η^1 perchlorate structure was identified at a lower energy than the chelating η^2 form, and was shown to be a true minimum (all frequencies were real). This monocoordinate η^1 alternative was recalculated for the Na^+ case. An alternative minimum energy structure was identified, but for **1**·$Na^+ClO_4^-$, this monocoordinate η^1 form was higher in energy then the chelating η^2 coordination mode (Na^+ series: monocoordinate η^1 perchlorate ion: –1663.3681640 Ha; chelating η^2 perchlorate ion: –1663.3756183 Ha). The larger K^+ ion allows space for the chelating η^2 perchlorate ion to be displaced towards one side of the crown. This unsymmetrical alternative had a lower energy than the symmetrical structure and was confirmed as a true minimum by frequency calculation. The symmetrical structure corresponds to an intermediate point between two lower energy conformations with the perchlorate offset to the left or to the right of the centre line of the crown ether. Comparing these three minimum energy structures, as expected, the smaller lithium ion dropped down closer to the mean plane of the oxygen atoms and the mean lithium–oxygen distance was shortened. The distances between the oxygen atoms in the crowns and the three alkali metal cations were compared. The Li–O(4) and Li–O(8) distances were shorter than in the DFT results for the sodium adduct. The potassium ion is easily large enough to coordinate to all five oxygen atoms, and lay significantly above the crown (mean M^+–O bond lengths by DFT: Li^+ 2.26; Na^+ 2.45; K^+ 2.76 Å). In each case, however, the shortest M^+–O distance was observed at O(6) at the centre of the more flexible CH_2–O(5)–CH_2–CH_2–O(6)–CH_2–CH_2–O(7)–CH_2 section of the crown where the ring can pucker more easily to allow O(6) to close up to the metal cation. The data obtained by DFT calculations provides a good basis to compare the different influences of M^+ ClO_4^- adducts on the IR vibrational modes of the

Table 3. Comparison of X-ray (M^+ = Na^+) and DFT (M^+ = Li^+, Na^+ and K^+) data for **1**·M^+ (DFT calculations were performed with perchlorate counterions for comparison with the coordination mode observed in the dimeric bridge related by a crystallographic centre in the X-ray structure of **1**·$M^+ClO_4^-$).

Selected bond lengths, angles and means							
Entry	M^+ anion	X-ray data[a] Na^+ SCN^-	X-ray data Na^+ ClO_4^-	DFT data Li^+ ClO_4^-	DFT data Na^+ ClO_4^-	DFT data K^+ ClO_4^-	Unit
1	M^+–O(4)	2.422(6)[b]	2.509(3)[b]	2.248(5)[b][c]	2.441(2)[b][c]	2.758(5)[b][c]	Å
2	M^+–O(5)	2.397(7)	2.469(4)	2.478(62)	2.503(2)	2.779(0)	Å
3	M^+–O(6)	2.351(7)	2.431(4)	2.090(0)	2.370(1)	2.711(2)	Å
4	M^+–O(7)	2.414(6)	2.414(3)	2.273(33)	2.503(0)	2.821(5)	Å
5	M^+–O(8)	2.422(6)	2.508(4)	2.206(18)	2.441(2)	2.719(2)	Å
6	mean M^+–O	2.401(14)	2.466(19)	2.259(74)	2.452(25)	2.758(21)	Å
7	C(4)–C(5)	1.399(12)	1.388(7)	1.412(0)	1.414(0)	1.417(0)	Å
8	C(5)–C(6)	1.418(13)	1.412(7)	1.434(1)	1.434(0)	1.433(0)	Å
9	C(6)–C(7)	1.391(14)	1.376(8)	1.411(0)	1.411(0)	1.411(0)	Å
10	C(7)–C(8)	1.389(14)	1.408(8)	1.435(0)	1.434(0)	1.432(0)	Å
11	C(8)–C(9)	1.395(11)	1.399(6)	1.412(0)	1.414(0)	1.417(0)	Å
12	mean (short)	1.395(3)	1.388(7)	1.412(0.3)	1.413(1)	1.415(2)	Å
13	mean (long)	1.404(15)	1.401(2)	1.435(1)	1.434(0)	1.433(0.5)	Å
14	C(4)–C(9)	1.415(11)	1.410(6)	1.440(0)	1.447(0)	1.449(0)	Å
15	C(4)–Cr–C(1)	89.7(4)	88.85(18)	90.76(3)	91.56(14)	92.04(25)	°
16	C(9)–Cr–C(1)	88.8(4)	88.12(18)	89.68(3)	91.56(21)	92.41(20)	°
17	mean C–Cr–C	89.25(45)	88.49(37)	90.22(54)	91.56(18)	92.23(21)	°
Selected nonbonding distances and angles between atoms							
18	O(4)···O(8)			2.562(2)	2.634(0)	2.713(0)	Å
19	C(1)···C(2)			2.590(1)	2.582(0)	2.578(1)	Å
20	C(1)···C(3)			2.590(1)	2.582(1)	2.577(0)	Å
21	mean C···C			2.590(1)	2.582(1)	2.578(1)	Å

[a] Data taken from ref.[8] [b] The error in the last significant figure is indicated by the value given in parenthesis. [c] The error was estimated by comparing the values obtained using Gaussian03 and Gaussian09 for the same functional (b3ylp) and basis set (Lanl2DZ).

$Cr(CO)_3$ complexes, and in this case has advantages over the use of data from crystallography. Our structure of $(\mathbf{1}{\cdot}Na^+ClO_4^-)_2$ is complicated by the dimeric coordination of the perchlorate ions. Crystallographically defined potassium 15-crown-5 adducts are typically[25] 2:1 complexes with K^+ lying between the two crowns, and in the only available crystal structure[26] of a lithium adduct of benzo-15-crown-5, the lithium ion is not situated in the crown at all, but is coordinated by a bidentate picrate ion and two water molecules.

The orientation of the tricarbonylchromium used in the DFT calculations was the same as that in the crystal structure in Figure 1 (a), and was retained in the optimised geometry. One unique carbonyl ligand [C(1)=O(1)] lies directly below the C(4)–C(9) bond of the arene that lies within the circumference of the crown. Although this is not the conformation observed in the structure[27] of **4**, there is considerable variation in the crystallographically defined conformations[28] of 1,2-disubstituted η^6 arene complexes, and in solution, free rotation of the $Cr(CO)_3$ group is expected. The orientation used in the calculations is convenient to allow a direct comparison with X-ray data for $\mathbf{1}{\cdot}Na^+$. The data in Table S3 (see Supporting Information) shows very little variation in the calculated Cr–CO and CrC–O bond lengths. The slight lengthening trend in the Cr–C(1) bond length for the unique CO ligand is matched by a compensating shortening of the C(1)–O(1) bond [Cr–C(1)/C(1)–O(1) 1.826/1.190 Å (for Li^+); 1.831/1.189 Å (for Na^+); 1.833/1.188 Å (for K^+)], but does not match the sequence of vibrational frequencies of ν_{sym} (Table 1). The origin of the changes revealed by PCA must be more subtle than a simple charge-based effect on the back-donation into the π* CO orbital.

The C–C bond lengths around the benzene ring show a pronounced alternating pattern[29] (lines 7–11, Table 3) but for the bonds in unsubstituted positions, there is very little variation with the nature of the alkali metal cation. The C(4)–C(9) bond length between the C–O bonds connecting the crown, however, is noticeably longer than the others and gradually lengthens as the size of the coordinated cation increases. The means of the C(4)–O(8) and C(9)–O(4) bond lengths similarly lengthen in the order $Li^+ > Na^+ > K^+$, indicating a decrease in π overlap in the O–C=C–O ↔ O=C–C=O benzo section of the crown for K^+. As would be expected, this change is more apparent in the distance between O(4) and O(8) [with Li^+: 2.562 Å; with Na^+: 2.634 Å; and with K^+: 2.713 Å, a range of 0.151 Å]. The entire O(4)–C(9)–C(4)–O(8) section of the benzo-15-crown-5 ligand is more compact with lithium in the crown and broader with potassium in the crown, with the dimensions for sodium lying somewhere in between. The consequence of this difference can be identified in the bonding to the unique carbonyl ligand that lies below C(4)–C(9). The C(4)–Cr–C(1) and C(9)–Cr–C(1) angles (Table 3, lines 15 and 16) increase in the sequence $Li^+ > Na^+ > K^+$, and the separation between the carbonyl ligand C(1)=O(1) and the other two C=O ligands (Table 3, lines 19 and 20) decreases. This can be illustrated by plotting C(4/9)–Cr–C(1) mean angles against the mean separation of C(1) from C(2/3) (Figure 8). The distance between C(2) and C(3) in contrast, hardly changes at all, and if anything, slightly increases. It is C(1) that is moving towards C(2/3), not the entire tripod of the $Cr(CO)_3$ narrowing [this same effect is apparent by comparing bond angle C(1)–Cr–C(2/3) which gets narrower, with C(2)–Cr–C(3) which is unchanged]. Hunter has shown[30] that in substituted (η^6-arene)$Cr(CO)_3$ complexes, the $Cr–C_{ipso}$ bond length is very sensitive to the π-donor/π-acceptor properties of the substituents on the arene. The mean values for the Cr–C(4) and Cr–C(9) bond lengths for the Li^+, Na^+ and K^+ complexes of **1** were also examined and show a declining trend (Li^+: 2.377; Na^+ 2.368; K^+ 2.363 Å), but the data do not correlate so well with the C(4/9)–Cr–C(1) bond angle as does the position of the C(1)=O(1) ligand. On this basis we propose that the main consequence of variation of M^+ in the crown is a splaying out of the entire [O(4)–C(9)–C(4)–O(8)]Cr–C(1)=O(1) section of the (benzo-15-crown-5)$Cr(CO)_3$ complex, and that this is more significant than a simple change in the π-donor/π-acceptor properties of the two crown oxygens attached to the η^6 arene ligand.

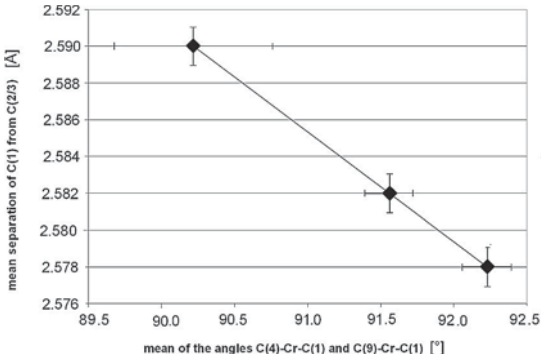

Figure 8. Plots of the means of the distances between C(1) and C(2) and between C(1) and C(3) (Table 3, line 21) against the mean of the angles C(4)–Cr–C(1) and C(9)–Cr–C(1) (Table 3, line 17).

The extent of changes of geometry in this section of the complex can be visualised (Figure 9) by considering an O(4)–O(8)–C(1)-based pyramid formed by extrapolating the bonds O(8)–C(4), O(4)–C(9) and O(1)–C(1) towards the centre line of the benzo-15-crown-5 ligand lying between C(6)–C(5)–C(4) and C(7)–C(8)–C(9). The narrower O(4)–O(8)–C(1)-based pyramid (Figure 9, a) observed for Li^+ corresponds to the longer Cr–C(4/9) distance which on the basis of Hunter's conclusions should suggest good π donation from O(4/8) into the aromatic ring. This pulling in of the C(1)≡O(1) carbonyl ligand could be a consequence of increased electron density in a bonding orbital in the space between Cr–C(1)–O(1), C(4/9) and O(4/8). With Na^+ in the crown, the metal cation is much better aligned with the sp^2 lone pairs on O(4/8), reducing the electron density on the oxygen atoms and so reducing π donation. Cr–C(4/9) shortens and the pyramid broadens as the C≡O ligand moves away from C(4)–C(9)·K^+ lies further above the crown which is bent back towards the $Cr(CO)_3$ group to a far

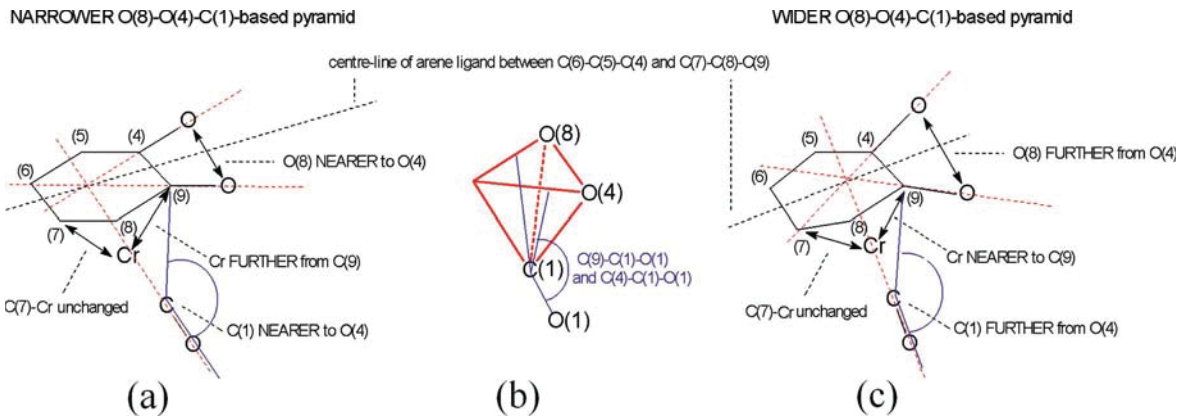

Figure 9. a: illustration of distortion of [O(4)–C(9)–C(4)–O(8)]Cr–C(1)=O(1) to form a narrower pyramid; b: the pyramid formed by extrapolating the bonds O(8)–C(4), O(4)–C(9) and O(1)–C(1) towards the centre line between the C(6)–C(5)–C(4) and C(7)–C(8)–C(9) sections of the arene ligand, and the angles C(9)–C(1)–O(1) (at the front of the pyramid) and C(4)–C(1)–O(1) (at the back of the pyramid); c: illustration of distortion of [O(4)–C(9)–C(4)–O(8)]Cr–C(1)=O(1) to form a wider pyramid.

greater extent than observed in the other two structures. Because of its larger size and its central position above the crown, orbitals on the potassium ion span O(4)–O(5)–O(6)–O(7)–O(8), and the K^+ ion can interact more with the π system of the benzocrown ligand than is the case with the smaller metal ions. This also reduces π donation into the arene ligand because donation to K^+ takes place instead. The distance between O(4) and O(8) widens in the presence of the larger metal ion, and the Cr–C(4/9) distance shortens further. Consequently the pyramid becomes still more splayed out (Figure 9, c). On this basis it is proposed that the qualitative influences on the IR spectra revealed by PCA are best explained by two different mechanisms: electronic effects are more significant with the π system in the case of K^+ but operate more through the σ bonds and the oxygen sp^2 lone pairs in the case of Na^+. For Li^+, the cation drops down more deeply into the crown, and so its effect by either mechanism on π donation into the arene ligand is less.

This proposal is supported by the presence of molecular orbitals that could account for the suggested interaction that pulls in the pyramid (Figure 10, a). The sodium ion crown complex (**1**·Na^+) was chosen to illustrate this because the arrangement of the seven oxygen atoms around the sodium ion (the five oxygen atoms of the crown and two from the perchlorate ion) in the energy minimum structure calculated by DFT was similar to that defined by crystallography. The filled molecular orbital 98 (–0.391 eV) for **1**·Na^+ has extensive contributions from orbital coefficients across the centre of the structure. Figure 10 (c) shows a lower energy filled orbital in which the π system of the carbonyl ligand that lies below the crown is distorted so that much of the electron density lies between the CO and the crown·Na^+ portions of the structure. These observations are consistent with the simple observation that ν_{sym} is shifted to higher wavenumbers when a cation coordinates the crown. This effect is much smaller with Li^+, which binds less readily. Although binding K^+ has the greatest effect on the geometry of the[O(4)–C(9)–C(4)–O(8)]Cr–C(1)=O(1) section of the (benzo-15-crown-5)$Cr(CO)_3$ complex, its affinity for the crown is less potent and its influence is similarly less than the effect of Na^+, which binds most strongly of the three cations studied here, and interacts with a better alignment with the oxygen lone pairs of the η^6-($H_4C_6O_2$) unit.

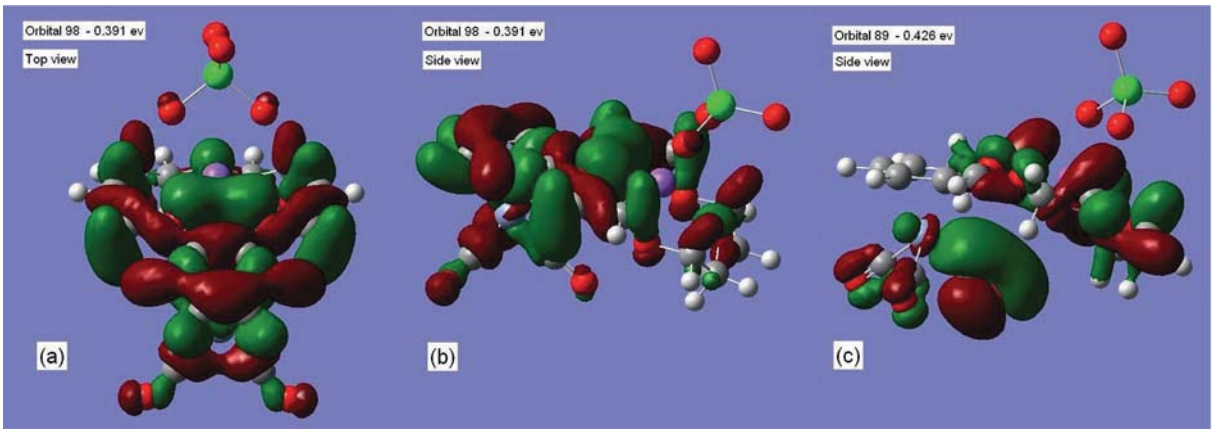

Figure 10. Images of molecular orbitals derived from DFT calculations on **1**·$Na^+C1O_4^-$: (a) orbital 98 (–0.391 eV); (b) side view of orbital 98; (c) orbital 89 (–0.426 eV).

Conclusions

Differences in the IR spectra of crown ether complexes of Li^+, Na^+, and K^+ ions can be qualitatively visualised by PCA and are a consequence of different contributions of charge- and orbital-based effects from Li^+, Na^+, and K^+ ions coordinated by the benzo-15-crown-5 ligand in the η^6 tricarbonylchromium derviative **1** used for FTIR studies. These effects are a consequence of structural changes in the [O(4)–C(9)–C(4)–O(8)]Cr–C(1)=O(1) section of the (η^6-benzo-15-crown-5)$Cr(CO)_3$ complex. Differences in the σ and π contributions influence the balance of the distribution of electron-density between the sp^2-hybridised oxygen atoms of η^6-($C_6H_4O_2$), the tricarbonylchromium arene complex and the coordinated metal ion. A wide range of cations influence the IR spectra of the ν(CO) stretching vibrations, but variation of the anion does not. Different tricarbonylchromium complexes respond to different M^+ ions to different extents and in different ways, which can be compared using ratios of $\Delta_{N(cation)}$ values, providing information needed for the design of dual probe methods for differential ion sensing by FTIR spectroscopy.

Experimental Section

General: The tricarbonylchromium complexes of crown ethers were prepared by a modification of the method of Mahaffey and Pauson.[31]

Tricarbonyl(η^6-1-pheny1-aza-15-crown-5)chromium(0) (2): A solution of 1-phenyl-1-aza-15-crown-5[32] (2.72 g, 9.22 mmol) and $Cr(CO)_6$ (1.50 g, 6.82 mmol) in a mixture of di-*n*-butyl ether (40 mL) and THF (4 mL) was heated under reflux for 48 h. The solution was filtered while hot, and the product precipitated on cooling. Recrystallisation from CH_2Cl_2/hexane yielded **2** as yellow crystals (1.22 g, 31%). ^{1}H NMR (270 MHz, [D_6]acetone): δ = 5.82 (dd,[33] $^3J_{H,H}$ = 7.2, 6.6 Hz, 2 H, H^{meta}), 5.13 (d, $^3J_{H,H}$ = 6.6 Hz, 2 H, H^{ortho}), 4.97 (t, $^3J_{H,H}$ = 7.2 Hz, 1 H, H^{para}), 3.77 (t, $^3J_{H,H}$ = 6.0, Hz, 4 H, OCH_2), 3.61 (s, 8 H, OCH_2), 3.55 (s, 4 H, OCH_2), 3.48 (t, $^3J_{H,H}$ = 6.0 Hz, 4 H, CH_2NCH_2) ppm. ^{13}C NMR (100 MHz, [D_6]acetone): δ = 236.3 $Cr(CO)_3$; 136.4 (C^{ipso}); 99.1 (C^{meta}); 83.7 (C^{para}); 76.6 (C^{ortho}); 71.8, 71.0, 70.7 (OCH_2CH_2O); 68.9 (OCH_2 adjacent to CH_2N–); 53.2 (CH_2NCH_2) ppm. IR (CH_2Cl_2): $\tilde{\nu}_{max}$ = 1967 (ν_{sym} CO), 1888 (ν_{asym} CO) cm^{-1}. MS (EI): *m*/*z* (%) = 431 [M^+]$^{\cdot}$, 347 [M – 3CO]$^{+\cdot}$, 319 [M – 3CO – CH_2CH_2]$^{+\cdot}$, 295 [M – $Cr(CO)_3$]$^{+\cdot}$, 289, 245, 201, 171, 157 (100), 143. HRMS (EI): *m*/*z* calcd. for $C_{19}H_{25}CrNO_7$ [M^+] 431.1036; found 431.1036. $C_{19}H_{25}CrNO_7$ (431.10): calcd. C 52.90, H 5.84, N 3.25; found C 52.71, H 5.84, N 3.18.

Tricarbonyl(η^6-2-phenyl-15-crown-5)chromium(0) (3): A solution of 2-phenyl-15-crown-5[34] (1.08 g, 3.65 mmol) and $Cr(CO)_6$ (0.85 g, 3.86 mmol) in a mixture of di-*n*-butyl ether (40 mL) and THF (4 mL) was heated under reflux for 48 h under an argon atmosphere. After cooling, the solution was filtered and the solvent removed in vacuo to give a yellow oil. Slow recrystallisation of the oil from CH_2Cl_2/hexane yielded **3** as a yellow solid (860 mg, 55%). ^{1}H NMR (270 MHz, [D_6]acetone): δ = 5.81 (d, $^3J_{H,H}$ = 6.3 Hz, 1 H, H^{ortho}), 5.76 (d, $^3J_{H,H}$ = 6.5 Hz, 1 H, H^{ortho}), 5.65 (t, $^3J_{H,H}$ = 6.2 Hz, 1 H, H^{para}), 5.58 (dd,[33] $^3J_{H,H}$ = 6.5, 6.2 Hz, 1 H, H^{meta}), 5.54 (dd,[33] $^3J_{H,H}$ = 6.5, 6.2 Hz, 1 H, H^{meta}), 4.38 (dd, $^3J_{H,H}$ = 5.4, 5.8 Hz, 1 H, CH), 3.88 and 3.63 (m, 18 H, OCH_2) ppm. ^{13}C NMR (100 MHz, [D_6]acetone): δ = 234.7 $Cr(CO)_3$; 112.9 (C^{ipso}); 95.8 (C^{para}); 93.2, 94.1 (C^{ortho}); 93.2, 93.1 (C^{meta}); 79.8 (2C); 75.8, (3C); 71.7, 71.5, 71.5, 71.3, 71.2, 71.2, 71.1 (–OCH_2CH_2O–) ppm. IR (CH_2Cl_2): $\tilde{\nu}_{max}$ = 1968 (ν_{sym} CO), 1889 (ν_{asym} CO) cm^{-1}. MS (EI): *m*/*z* (%) = 432 [M^+]$^{\cdot}$, 376 [M – 2CO]$^{+\cdot}$, 348 [M – 3CO]$^{+\cdot}$, 244, 200, 156 (100), 126, 96. $C_{19}H_{24}CrO_8$ (432.39): calcd. C 52.78, H 5.59; found C 53.11, H 5.40.

Crystallography: Data were measured at 298 K on a Siemens R3m/v 4-circle diffractometer using graphite-monochromated Mo-K_α radiation (λ = 0.71073 Å). Data were corrected for absorption using ψ-scans. Structure solution by Patterson synthesis and full-matrix least-squares refinement of the structure (against F^2, all data) were carried out using the SHELXTL software package.[35] The oxygens of the perchlorate anion was found to be disordered twofold; the components were refined with 82% and 18% occupancies, but from the thermal parameters the presence of further unresolved disorder is likely. All non-hydrogen atoms (except the minor components of the disordered oxygen atoms) were refined anisotropically, and the methylene hydrogen atoms were placed in calculated positions.

[(1·Na^+)ClO_4^-]$_2$: $C_{34}H_{40}Cl_2Cr_2Na_2O_{24}$, 1053.54 g mol^{-1}, monoclinic, *C2*/*c*, *a* = 27.959(7), *b* = 10.367(3), *c* = 16.660(4) Å, β = 117.712(19)°, *V* = 4275(2) Å^3, *T* = 293(2) K, *F*(000) = 2160, d_{calc} = 1.637 g cm^{-3}, μ(Mo-K_α) = 0.743 mm^{-1}. 3711 data collected, of which 3638 unique (R_{int} = 0.0213), 306 parameters, final wR_2 = 0.1111, *S* = 1.013 (all data), R_1 = 0.0464 [2627 with $I > 2\sigma(I)$], largest final difference peak/hole = +0.318/–0.460 e Å^{-3}.

Crystallographic data (excluding structure factors) for [(**1**·Na^+)-$C1O_4^-$]$_2$ have been deposited with the Cambridge Crystallographic Data Centre as supplementary publication number CCDC-745686. These data can be obtained free of charge from The Cambridge Crystallographic Data Centre via www.ccdc.cam.ac.uk/data_request/cif. The structure of (**1**·Na^+)SCN^- was deposited previously at CCDC with the refcode POGZAM.[8]

Spectroscopic Measurements: FTIR spectra were measured at 0.5 cm^{-1} resolution using a 0.5 mm pathlength CaF_2 solution cell and a Perkin–Elmer 1720X spectrometer equipped with a liquid nitrogen-cooled InSb detector (an attenuation filter was used to avoid detector saturation); 16 scans were collected for each spectrum. The temperature in the IR beam at the sample position during scanning was in the range 298–300 K. For the PCA experiments, stock solutions of metal salts in dry methanol were made up to volumes of 10 mL. For a given spectrum, 0.2 mL of a stock solution of the chromium complex was added to a 2 mL portion of a salt solution. The samples for the surveys of cations (NH_4^+, Li^+, Na^+, K^+, Rb^+, Cs^+, Mg^{2+}, Ba^{2+}) and anions (AcO^-, BPh_4^-, Br^-, $C1O_4^-$, I^-, SCN^-) were prepared similarly, using stock solutions of the salts at higher concentrations such that the final concentrations of salt and chromium complex were as given in the text. The spectrum of each solution was measured immediately after mixing; provided bright light was avoided, no measurable oxidative decomposition of the complexes was noted for at least 20 min, even when air-containing solvents were employed. Since the bandshapes for the ν_{asym}(CO) modes were generally rather unsymmetrical, the wavenumber of the mode was calculated by measuring the positions in wavenumbers on either side of the band at the points where the absorbance was half that at the band maximum. The mean of these two values used to estimate the wavenumber of the centre of the antisymmetric band envelope.

DFT Calculations: The X-ray coordinates of tricarbonylchromium η^6-benzocrown portion of the published[8] structure of **1**·Na^+ SCN^- salt were taken as the starting point[36] for the geometry optimis-

ation of the perchlorate with the η^2 O–Na–O perpendicular to the centre-line of the benzocrown, using the b3ylp functional[37] and the Lanl2DZ basis set[38] as implemented by Gaussian03. The optimisation was repeated using the b3ylp/Lanl2DZ/Gaussian09.[39] The resulting geometry was used in optimisations of the **1**·Li^+ and **1**·K^+ coordination complexes. Frequency calculations made at the same level showed that all the frequencies are real, thus the four optimised structures each correspond to local energy minima. The distance and angle data (from Gaussian09/Molden[40]) and structural and molecular orbital (MO) images (from Gaussian03[41]/Gaussview[42]) are presented in Table 3, Figures 1 and 10. The full tables for the optimised geometries of **1**·Li^+ ClO_4^-, **1**·Na^+ ClO_4^-, and **1**·K^+ ClO_4^- are presented in the Supporting Information.

Supporting Information (see footnote on the first page of this article): FTIR plots and tabulations, comparison of DFT and crystallographic data, and DFT-derived atom coordinates and orbital energies.

Acknowledgments

We thank the EPSRC National Mass Spectrometry Service (Swansea University) for high resolution mass data, Dr J. Varga and Dr J. Lejtovicz [Central Research Institute (CRI) of the Hungarian Academy of Sciences] for use of the PCCAP software, and Dr O. Egyed (CRI) for discussions. G. R. S. and C. A. D. thank the European Union (EU COST programme) for financial support

[1] For recent examples of conventional strategies, see: a) J. Gao, S. Rochat, X. Quan, K. Severin, *Chem. Eur. J.* **2010**, *16*, 5013–5017 (lithium ions); b) A. Nierth, A. Y. Kobitski, G. U. Nienhaus, A. Jaschke, *J. Am. Chem. Soc.* **2010**, *132*, 2646–2658; c) G. Mirri, S. D. Bull, P. N. Norton, T. D. James, L. Male, J. H. R. Tucker, *J. Am. Chem. Soc.* **2010**, *132*, 8903–8905; d) J. Estban, J. Vincente, R. Martínez-Máñez, M. D. Marcos, M. Moragues, J. Soto, F. Sancenón, *Angew. Chem. Int. Ed.* **2010**, *49*, 49434–4937; e) G. Fukuhara, Y. Inoue, *Chem. Eur. J.* **2010**, *16*, 7859–7864; f) L. Feng, C. J. Musto, K. S. Suslick, *J. Am. Chem. Soc.* **2010**, *132*, 4046–4047; g) Y. H. Lee, H. Lui, J. Y. Lee, S. H. Kim, S. K. Kim, J. L. Sessler, Y. Kim, J. S. Kim, *Chem. Eur. J.* **2010**, *16*, 5895–5901; h) N. Laurieri, M. H. J. Crawford, A. Kawamura, I. M. Westwood, J. Robinson, A. M. Fletcher, S. G. Davis, E. Sim, A. J. Russell, *J. Am. Chem. Soc.* **2010**, *132*, 3238–3239; i) R. Hu, J. Feng, D. Hu, S. Wang, S. Li, G. Yang, *Angew. Chem. Int. Ed.* **2010**, *49*, 4915–4918; j) F. Westerlund, C. B. Hildebrandt, T. J. Sørensen, B. W. Laursen, *Chem. Eur. J.* **2010**, *16*, 2992–2996; k) J. J. Gassensmith, S. Matthys, J.-J. Lee, A. Wojcik, P. V. Mamat, B. D. Smith, *Chem. Eur. J.* **2010**, *16*, 2916–2921; l) A. N. Swinburne, M. J. Patterson, K. H. Fischer, S. J. Dickson, E. V. B. Wallace, W. J. Belcher, A. Beeby, J. W. Steede, *Chem. Eur. J.* **2010**, *16*, 1480–1492; m) H.-L. Liu, Q. Peng, Y.-D. Wu, D. Chen, X.-L. Hou, M. Sabat, L. Pu, *Angew. Chem. Int. Ed.* **2010**, *49*, 602–606; for reviews on fluorescence, see: n) I. Leray, B. Valeur, *Eur. J. Inorg. Chem.* **2009**, 3525–3535; o) D. Patra, A. K. Mishra, *Encyclopedia Sensors* **2006**, *2*, 139–156; p) L. Prodi, M. Montali, N. Zaccheroni, L. Dolci, S. Luisa, *Top. Fluoresc. Spectrosc.* **2005**, *9*, 1–57; q) A. P. Demchenko, *Anal. Biochem.* **2005**, *343*, 1–22; r) P. B. Oldham, M. E. McCarroll, L. B. McGown, I. M. Warner, *Anal. Chem.* **2000**, *72*, 197–209; s) B. Valeur, I. Leray, *Coord. Chem. Rev.* **2000**, *205*, 3–40. UV: t) R. Jelinek, *Drug Dev. Res.* **2000**, *50*, 497–501; for reviews on electrochemistry, see: u) R. M. El Nashar, H. A. A. Wagdy, H. Y. Abdoul-Enein, *Curr. Anal. Chem.* **2009**, *5*, 249–270; v) M. Trojanowicz, M. Kaniewska, *Electroanalysis* **2009**, *21*, 229–238; w) P. Milina, A. Tarraga, A. Caballero, *Eur. J. Inorg. Chem.* **2008**, 3401–3417; x) S. R. Bayly, P. D. Beer, G. Z. Chen, *Ferrocenes* **2008**, 281–318.

[2] For a review on the organometalcarbonyl probe approach, see: a) G. R. Stephenson, *Organometallic Bioprobes* in *Bioorganometallic Chemistry* (Ed.: G. Jaouen), Wiley-VCH, Weinheim, Germany, **2005**, p. 215–262 (ISBN 3-527-30990-X); for a recent example using Raman spectroscopy, see: b) K. Meister, J. Nielson, U. Schatzschneider, N. Metzler-Nolte, D. A. Schmidt, M. Havenith, *Angew. Chem. Int. Ed.* **2010**, *49*, 3310–3312; see also: c) C. E. Anson, C. S. Creaser, O. Egyed, G. R. Stephenson, *Spectrochim. Acta* **1997**, *53A*, 1867–1877; d) C. E. Anson, C. S. Creaser, J. A. Downie, O. Egyed, A. V. Malkov, L. Mojovic, G. R. Stephenson, A. T. Turner, K. E. Wilson, *Bioorg. Med. Chem. Lett.* **1998**, *8*, 3549–3554; for Jaouen and Vessieres' pioneering studies in CMIA, see: e) G. Jaouen, A. Vessieres, *Pure Appl. Chem.* **1989**, *61*, 565–572; f) M. Salmain, A. Vessieres, I. S. Butler, G. Jaouen, *Bioconjugate Chem.* **1991**, *2*, 13–15; g) M. Salmain, A. Vessieres, I. S. Butler, G. Jaouen, *Anal. Chem.* **1991**, *63*, 2323–2329; for other recent examples, see: h) M. Salmain, A. Vessieres, *Bioorganometallics* **2006**, 263–302; i) N. Fischer-Durand, A. Vessieres, J.-M. Heldt, F. le Bideau, G. Jaouen, *J. Organomet. Chem.* **2003**, *668*, 59–66; j) M. Salmain, N. Fischer-Durand, L. Cavalier, B. Rudolf, J. Zakrewski, G. Jaouen, *Bioconjugate Chem.* **2002**, *13*, 693–698; for approaches to DNA sensing, see: k) K. Kowalski, J. Zakrzewski, *J. Organomet. Chem.* **2003**, *668*, 91–94; for early applications with surface amino groups on proteins, see: l) C. E. Anson, C. S. Creaser, O. Egyed, M. A. Fey, G. R. Stephenson, *J. Chem. Soc., Chem. Commun.* **1994**, 39–40; for an example of organometallic derivatives of amino acids, see: m) M. J. Dunn, R. F. W. Jackson, G. R. Stephenson, *Synlett* **1992**, 905–906.

[3] C. S. Creaser, W. E. Hutchinson, G. R. Stephenson, *Appl. Spectrosc.* **2000**, *54*, 1624–1628.

[4] K. H. Pannell, D. C. Hambrick, G. S. Lewandos, *J. Organomet. Chem.* **1975**, *99*, C21–C23.

[5] K. J. Odell, E. M. Hyde, B. L. Shaw, I. Shepherd, *J. Organomet. Chem.* **1979**, *168*, 103–114.

[6] C. Baldoli, P. Del Buttero, S. Maiorana, A. Papagni, *J. Chem. Soc., Chem. Commun.* **1985**, 1181–1182.

[7] For 4-methylanilinium binding to an η^4-$Fe(CO)_3$ complex of a benzocrown ether, see: H. Yamaguchi, S. Nakanishi, N. Kilhara, T. Takata, *Tetrahedron Lett.* **2001**, *42*, 1699–1702.

[8] C. E. Anson, C. S. Creaser, G. R. Stephenson, *J. Chem. Soc., Chem. Commun.* **1994**, 2175–2176.

[9] a) A. P. de Silva, H. Q. Gunarante, T. Gunnlaugsen, A. J. Huxley, C. P. McCoy, J. T. Rademacher, T. E. Rice, *Chem. Rev.* **1997**, *97*, 1515–1566; b) for a fluorescence-based array sensor approach, see: Y. Liu, M. A. Palacos, P. Anzenbacher, *Chem. Commun.* **2010**, 1860–1862; c) for two-photon imaging, see: M. K. Kim, C. S. Lim, J. T. Hong, J. H. Han, H.-Y. Jang, H. M. Kim, B. R. Cho, *Angew. Chem. Int. Ed.* **2010**, *49*, 364–367.

[10] Li^+- and Na^+-induced shifts in ν(CO) have been reported for an η^5 $Mn(CO)_3$ analogue: H. Plenio, D. Burth, *Organometallics* **1996**, *15*, 1151–1156.

[11] E. Peris, J. A. Mata, V. Moliner, *J. Chem. Soc., Dalton Trans.* **1999**, 3893–3898.

[12] C. E. Anson, T. J. Baldwin, C. S. Creaser, M. A. Fey, G. R. Stephenson, *Organometallics* **1996**, *15*, 1451–1456.

[13] K. Kowalski, R. F. Winter, A. Makal, A. Pazio, K. Wozniak, *Eur. J. Inorg. Chem.* **2009**, 4069–4077.

[14] C. S. Creaser, M. A. Fey, G. R. Stephenson, *Spectrochim. Acta Part A* **1994**, *50*, 1295–1299.

[15] L. J. Bellamy, R. L. Williams, *J. Chem. Soc.* **1957**, 863–868.

[16] C. E. Anson, T. J. Baldwin, N. J. Clayden, C. S. Creaser, O. Egyed, M. A. Fey, W. E. Hutchinson, A. Kavanagh, G. R. Stephenson, P. I. Walker, *J. Optoelectronics Adv. Mater.* **2003**, *5*, 533–554.

[17] J. Varga, J. Lejtovicz, unpublished software.

[18] The multiple sensor approach uses several complexes with non-overlapping vibrational bands in the same spectroscopic experiment to gain extra information about a single analyte, or simultaneous information about several analytes. For examples of

dual probes with mixed solvents and for pH measurement, see: a) C. S. Creaser, W. E. Hutchinson, G. R. Stephenson, *Analyst* **2001**, *126*, 647–651, and ref.[12]; for examples of multiple probes in CMIA, see: b) M. Salmain, A. Vessieres, P. Brossier, G. Jaouen, *J. Organomet. Chem.* **1999**, *589*, 92–97; c) M. Salmain, A. Varrene, A. Vessieres, G. Jaouen, *Appl. Spectrosc.* **1998**, *52*, 1382–1390; d) A. Varrene, A. Vessieres, M. Salmain, S. Durand, P. Brossier, G. Jaouen, *Anal. Biochem.* **1996**, *242*, 172–179.

[19] C. E. Anson, C. S. Creaser, G. R. Stephenson, *Spectrochim. Acta* **1996**, *52A*, 1183–1191.

[20] For an example of an η^6-arylruthenium complex of (benzo-15-crown-5)**1**·Na^+, see: D. S. Perekalin, M. V. Babak, V. V. Novikov, K. A. Lyssenko, M. Corsin, P. Zanello, A. R. Kudinov, *J. Organomet. Chem.* **2010**, *695*, 1200–1204.

[21] J. D. Owen, *J. Chem. Soc., Dalton Trans.* **1980**, 1066–1075.

[22] a) J. Tao, K. Ding, Y. Zhu, *Chin. J. Chem.* **1992**, *10*, 513–518; b) S. Appel, F. Weller, K. Dehneicke, *Z. Anorg. Allg. Chem.* **1990**, *583*, 7–16; c) Z. Zhou, X. Xang, L. Ye, Y. Fan, *Wuji Huaxue Xuebao* **1990**, *6*, 433–438 (*Chem. Abstr.* **1991**, *115*, 293490); d) H. Borgholte, K. Dehnicker, H. Goesmann, D. Fenske, *Z. Anorg. Allg. Chem.* **1990**, *586*, 159–165; e) W. A. Herrmann, J. G. Kucher, G. Weischelbaumer, E. Hertweck, P. Kiprof, *J. Organomet. Chem.* **1989**, *372*, 351–370; f) D. L. Ward, A. J. Popov, N. S. Poonia, *Acta Crystallogr., Sect. C* **1984**, *40*, 238–241; g) I. R. Hanson, D. G. Parsons, M. R. Truter, *Acta Crystallogr., Sect. B* **1982**, *38*, 448–451; h) D. C. Moody, R. R. Ryan, *Cryst. Struct. Commun.* **1979**, *8*, 993–936; i) M. A. Bush, M. R. Truter, *J. Chem. Soc. Perkin Trans. 1* **1972**, 341–344.

[23] For an example of a DFT study of an η^6-arylcobalt complex of (benzo-15-crown-5)**1**·Na^+, see: D. S. Perekalin, M. V. Babak, V. V. Novikov, P. V. Petrovskii, K. A. Lyssenko, M. Corsin, P. Zanello, A. R. Kudinov, *Organometallics* **2008**, *27*, 3654–3658.

[24] For recent examples of DFT calculations on crown ether complexes, see: a) B. Martinez-Haya, P. Hurtado, A. R. Hortal, S. Hamad, J. D. Steill, J. Oomens, *J. Phys. Chem. A* **2010**, *114*, 7048–7054; b) R. Bandyopadhyay, B. F. T. Cooper, A. J. Rossini, R. W. Schurko, C. L. B. MacDonnald, *J. Organomet. Chem.* **2010**, *695*, 1012–1018; c) X. Zheng, X. Wanf, S. Yi, N. Wang, Y. Peng, *J. Comput. Chem.* **2009**, *30*, 2674–2683; d) K.-S. Daio, H.-J. Weang, Z.-M. Qui, *J. Solution Chem.* **2009**, *39*, 713–724; e) M. D. Brown, M. F. Davis, J. M. Dyke, F. Ferrante, W. Levason, S. J. Ogden, M. Webster, *Chem. Eur. J.* **2008**, *14*, 2615–2624; f) for our results on decaoxaspherophanes, see: A. Saal, T. Jarrosson, O. Ouamerali, C. A. Daul, *Chem. Phys. Lett.* **2009**, *480*, 225–230; g) for applications of DFT in inorganic and analytical chemistry, see: C. A. Daul, *Chimia* **1994**, *48*, 343–347.

[25] a) A. Mugnoli, Z. Dauter, E. Luboch, A. Cygan, J. F. Biernat, *J. Inclusion Phenom.* **1986**, *4*, 407–414; b) W. S. Sheldrick, N. S. Poonia, *J. Inclusion Phenom.* **1986**, *4*, 93–98; c) V. W. Bhagwat, H. Manohar, N. S. Poonia, *Inorg. Nucl. Chem. Lett.* **1981**, *17*, 207–210; d) P. R. Mallinson, M. R. Truter, *J. Chem. Soc. Perkin Trans. 2* **1972**, 1818–1823.

[26] V. W. Bhagwat, H. Manohar, N. S. Poonia, *Inorg. Nucl. Chem. Lett.* **1980**, *16*, 373–375.

[27] J. C. Boutonnet, F. Rose-Munch, E. Rose, Y. Jeannin, F. Robert, *J. Organomet. Chem.* **1985**, *297*, 185–194.

[28] a) Y. Dusausoy, J. Protas, J. Besancon, S. Top, *J. Organomet. Chem.* **1975**, *94*, 47–53; b) P. Berno, A. Ceccon, A. Gambaro, A. Venzo, P. Ganis, G. Vaille, *J. Chem. Soc. Perkin Trans. 1* **1987**, 935–941; c) T. G. Traylor, M. J. Goldberg, A. R. Miksztal, C. E. Strouse, *Organometallics* **1989**, *8*, 1101–1105; d) E. P. Kundig, C. Grivet, E. Wenger, G. Bernarddinelli, A. F. Williams, *Helv. Chim. Acta* **1991**, *74*, 2009–2023; e) M. Brands, R. Goddard, H. G. Wey, H. Butenschön, *Angew. Chem. Int. Ed. Engl.* **1993**, *32*, 267–269.

[29] a) B. P. Byers, M. P. Hall, *Organometallics* **1987**, *6*, 2319–2325; b) E. L. Meutterties, J. R. Bleeke, E. J. Wucherer, A. T. Albright, *Chem. Rev.* **1982**, *82*, 499–525; c) T. A. Albright, *Acc. Chem. Res.* **1982**, *15*, 149–155.

[30] a) A. D. Hunter, L. Shilliday, W. L. Furey, M. J. Zaworotko, *Organometallics* **1992**, *11*, 1550–1556; b) A. D. Hunter, V. Mozol, S. D. Tsai, *Organometallics* **1990**, *11*, 2251–2262.

[31] C. A. L. Mahaffey, P. L. Pauson, *Inorg. Synth.* **1979**, *19*, 154–158.

[32] a) X.-X. Zhang, S. L. Buchwald, *J. Org. Chem.* **2000**, *65*, 8027–8031; b) J. P. Dix, F. Voegtle, *Chem. Ber.* **1980**, *113*, 457–470.

[33] The multiplet was not fully resolved and appeared as an apparent triplet; the coupling constants are inferred from signals for adjacent hydrogen atoms.

[34] B. R. Bowsher, A. J. Rest, B. G. Main, *J. Chem. Soc., Dalton Trans.* **1984**, 1421–1425.

[35] G. M. Sheldrick, *Acta Crystallogr., Sect. A* **2008**, *64*, 112–122.

[36] For an example of this approach, see: C.-C. Su, *J. Mol. Struct.* **2008**, *892*, 231–238.

[37] A. D. Becke, *J. Chem. Phys.* **1993**, *98*, 5648–5652.

[38] P. J. Hay, W. R. Wadt, *J. Chem. Phys.* **1985**, *82*, 270–298; P. J. Hay, W. R. Wadt, *J. Chem. Phys.* **1985**, 82; P. J. Hay, W. R. Wadt, *J. Chem. Phys.* **1985**, 299–310.

[39] M. J. Frisch, G. W. Trucks, H. B. Schlegel, G. E. Scuseria, M. A. Robb, J. R. Cheeseman, G. Scalmani, V. Barone, B. Mennucci, G. A. Petersson, H. Nakatsuji, M. Caricato, X. Li, H. P. Hratchian, A. F. Izmaylov, J. Bloino, G. Zheng, J. L. Sonnenberg, M. Hada, M. Ehara, K. Toyota, R. Fukuda, J. Hasegawa, M. Ishida, T. Nakajima, Y. Honda, O. Kitao, H. Nakai, T. Vreven, J. A. Montgomery Jr., J. E. Peralta, F. Ogliaro, M. Bearpark, J. J. Heyd, E. Brothers, K. N. Kudin, V. N. Staroverov, R. Kobayashi, J. Normand, K. Raghavachari, A. Rendell, J. C. Burant, S. S. Iyengar, J. Tomasi, M. Cossi, N. Rega, J. M. Millam, M. Klene, J. E. Knox, J. B. Cross, V. Bakken, C. Adamo, J. Jaramillo, R. Gomperts, R. E. Stratmann, O. Yazyev, A. J. Austin, R. Cammi, C. Pomelli, J. W. Ochterski, R. L. Martin, K. Morokuma, V. G. Zakrzewski, G. A. Voth, P. Salvador, J. J. Dannenberg, S. Dapprich, A. D. Daniels, Ö. Farkas, J. B. Foresman, J. V. Ortiz, J. Cioslowski, D. J. Fox, *Gaussian 09*, rev. A.1, Gaussian Inc., Wallingford CT, **2009**.

[40] G. Schaftenaar, J. H. Noordik, *J. Comput.-Aided Mol. Des.* **2000**, *14*, 123–134.

[41] M. J. Frisch, G. W. Trucks, H. B. Schlegel, G. E. Scuseria, M. A. Robb, J. R. Cheeseman, J. A. Montgomery Jr., T. Vreven, K. N. Kudin, J. C. Burant, J. M. Millam, S. S. Iyengar, J. Tomasi, V. Barone, B. Mennucci, M. Cossi, G. Scalmani, N. Rega, G. A. Petersson, H. Nakatsuji, M. Hada, M. Ehara, K. Toyota, R. Fukuda, J. Hasegawa, M. Ishida, T. Nakajima, Y. Honda, O. Kitao, H. Nakai, M. Klene, X. Li, J. E. Knox, H. P. Hratchian, J. B. Cross, V. Bakken, C. Adamo, J. Jaramillo, R. Gomperts, R. E. Stratmann, O. Yazyev, A. J. Austin, R. Cammi, C. Pomelli, J. W. Ochterski, P. Y. Ayala, K. Morokuma, G. A. Voth, P. Salvador, J. J. Dannenberg, V. G. Zakrzewski, S. Dapprich, A. D. Daniels, M. C. Strain, O. Farkas, D. K. Malick, A. D. Rabuck, K. Raghavachari, J. B. Foresman, J. V. Ortiz, Q. Cui, A. G. Baboul, S. Clifford, J. Cioslowski, B. B. Stefanov, G. Liu, A. Liashenko, P. Piskorz, I. Komaromi, R. L. Martin, D. J. Fox, T. Keith, M. A. Al-Laham, C. Y. Peng, A. Nanayakkara, M. Challacombe, P. M. W. Gill, B. Johnson, W. Chen, M. W. Wong, C. Gonzalez, J. A. Pople, *Gaussian 03*, rev. C.02, Gaussian Inc., Wallingford CT, **2004**.

[42] A. Frisch, R. D. Dennington II, T. A. Keith, *GaussView*, version 3.0, Gaussian Inc., Pittsburgh, PA, **2003**.